ISSN 0036-0244, Russian Journal of Physical Chemistry A, 2022, Vol. 96, No. 9, pp. 1935–1943. © Pleiades Publishing, Ltd., 2022.

CHEMICAL KINETICS AND CATALYSIS

Highly Efficient Hydrogen Production from Ammonia Borane over Carbon Nanotubes Supported Pt–Ni Bimetallic Catalyst

Hui Zhang[a,*], Jin He[a], Bowen Lei[a], Jie Wen[a,], Fangli Jing[a], and Arshid Mahmood Ali[b]**

[a] *Center for Computational Chemistry and Molecular Simulation, Oil and Gas Field Applied Chemistry Laboratory, College of Chemistry and Chemical Engineering, Southwest Petroleum University, Chengdu, 610500 China*

[b] *Department of Chemical and Materials Engineering, King Abdulaziz University, Jeddah, 21589 Saudi Arabia*

**e-mail: huizhang@swpu.edu.cn*

***e-mail: wenjie@swpu.edu.cn*

Received December 6, 2021; revised January 13, 2022; accepted January 17, 2022

Abstract—The bimetallic Pt–Ni nano-catalysts with different platinum to nickel mass ratios supported on the carbon nanotubes (PtNi(x : y)/FCNTs-D) were successfully synthesized by the polyol method and applied to the H_2 generation from ammonia borane (AB) hydrolysis. Several state-of-the-art characterization methods were performed to explore the correlation between catalytic performance and the physicochemical characterizations of the catalysts. The results show that the optimum Pt : Ni ratio is critical to enhance the H_2 generation from AB hydrolysis and in this study, it is 1 : 2. The presence of carbon nanotubes enhanced the dispersion and stability of the Pt–Ni nanoparticles. The availability of more active sites and lowered binding energy of Pt^0 in PtNi(1 : 2)/FCNTs-D catalyst, lead to the increased catalytic activity of H_2 generation from AB hydrolysis.

Keywords: bimetallic Pt–Ni nano-catalyst, carbon nanotubes, ammonia borane, hydrogen generation, catalytic hydrolysis

DOI: 10.1134/S0036024422090357

INTRODUCTION

Hydrogen, one of the cleanest fuels, has received a lot of attention [1]. However, the controlled storage and release of hydrogen is still a challenging issue [2]. In recent years, different materials have been developed for the storage of hydrogen such as metal organic framework materials (MOF-5) [3], metal hydrides ($LaNi_5H_6$, $NaAlH_4$, $LiAlH_4$, AlH_3) [4], borohydrides [5], organic liquid storage hydrogen materials [6] and ammonia borane (AB) [7]. Among them, solid ammonia borane, is regarded as potential hydrogen storage material [8] because of high-quality hydrogen storage density (19.6%) and high stability. In addition, the hydrogen stored in AB can be released through its hydrolysis at room temperature in the presence of a suitable catalyst.

Noble metal catalysts with high catalytic activity are commonly used catalysts for the hydrolysis of AB, among them Pt is the most active metals for AB dehydrogenation [9, 10]. Chen et al. reported Pt/CNT-O-HT catalyst for catalyzing the hydrolytic dehydrogenation of AB with TOF up to 567 $mol_{H_2}\ min^{-1}\ mol_{pt}^{-1}$. Because of depleting Pt sources and high price, the achieved excellent results are yet not conducive to practical applications. Therefore, an effective strategy is the combination of Pt with earth abundant transition metals [11]. The synergistic effect between different metal atoms can significantly improve the activity and selectivity of catalytic reactions [12, 13]. The Pt–Ni bimetallic nano-catalyst is considered to be one of the most potential catalysts in hydrogen generation AB hydrolysis. Thence, scientific design and controllable preparation of Pt–Ni bimetallic nano-catalyst are of great significance to the practical application of hydrogen production reaction system from AB. Moreover, the metal nanoparticles are often supported on the various carriers to avoid agglomeration and deactivation. In recent years, carbon materials with unique physical and chemical properties such as porous carbon, carbon nanotubes and graphene have been widely used as excellent carriers [14, 15]. In addition to the carbon materials, the metal nanoparticles were also supported on other metal oxides such as CeO_2, ZrO_2, HfO_2, and TiO_2, has also shown a good catalytic activity in AB hydrolysis.

Inspired by the above-described studies, we herein report a simple and convenient method for the design and synthesis of a bimetallic Pt–Ni nano-catalysts with different platinum to nickel mass ratios supported on the carbon nanotubes. The proposed preparation protocol of the PtNi(x : y)/FCNTs-D catalysts is out-

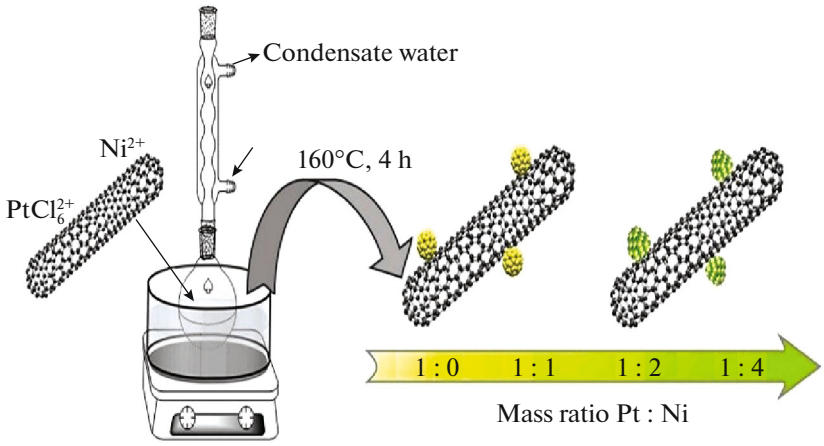

Fig. 1. Preparation sketch for PtNi(x : y)/FCNTs-D catalysts.

lined in Fig. 1. All the freshly prepared catalysts were tested based on their catalytic activity for AB hydrolysis. In addition, the effect of temperature to the catalytic activity of selected PtNi(1 : 2)/FCNTs-D catalyst for AB hydrolysis of AB is also studied. Based on initial assessments, the bimetallic Pt–Ni nano-catalysts supported on the carbon nanotubes can significantly improve the catalytic activity and the stability of the active center of the catalyst.

EXPERIMENTAL

Commercially available materials were used without further purification. Ethanol absolute (AR), acetone (AR), nickel chloride hexahydrate (AR), ethylene glycol (AR), and NaOH (AR) were purchased from Keshi. Ammonia borane (AB, 97%) and chloroplatinic acid hexahydrate (AR) were purchased from Aladdin. Carboxylated carbon nanotubes (L = 0.5–2 μm, D = 8–15 nm) was purchased from Timesnano. Deionized water was used for the preparation of metal precursor salt solution.

The PtNi(x : y)/FCNTs-D catalysts were prepared by the polyol method (see Fig. 1). For the catalyst synthesis, carboxylated carbon nanotubes (100 mg) was added to ethylene glycol (30 mL) solution. $H_2PtCl_6{\cdot}6H_2O$ (8 mg) and $NiCl_2{\cdot}6H_2O$ (12 mg) were added to the solution of ethylene glycol (20 mL). Later, the salt solution was added dropwise to the ethylene glycol dispersion containing carboxylated carbon nanotubes under continuous stirring conditions. After it, the mixture was sonicated for 30 min and kept under overnight stirring. The resultant reaction mixture's pH was adjusted to 11 after transferring it to 100 mL flask and kept reacting for 4 h at 160°C. Acetone was added to get precipitates and solid sample was obtained after centrifugal separation. The solid sample was multiply rinsed (3 times) by using a solvent composed of acetone and ethanol, then dried overnight under vacuum at 65°C to obtain the PtNi(1 : 1)/FCNTs-D catalyst. Similarly, the catalysts with different platinum-nickel ratios were prepared by changing the amount of nickel precursor salt and abbreviated as PtNi(x : y)/FCNTs-D.

The morphology structures of samples were characterized by transmission electron microscope (Hitachi-7700 TEM, Hitachi, accelerating voltage 100 kV). The XRD patterns of various catalysts were collected from a PANalytical X-ray powder diffractometer (XRD, X'Pert PRO MPD) using CuK_α radiation (λ = 1.5406 Å) over a scan range of 10°–80°. X-ray photoelectron spectroscopy (XPS) was acquired by Thermo VG ESCALAB 250 (Thermo Fisher Scientific, US) and the charge correction was performed at 284.5 eV of carbon. Fourier transform infrared spectroscopy (FT-IR) were collected on a WQF 520 (Beijing Ruili Analytical Instrument Co., Ltd.).

The catalytic activity tests for AB hydrolysis to hydrogen generation were carried in a device as shown in Fig. 2. 5 mg of the freshly prepared catalyst and 5 mL of deionized water was added into a 10 mL three-necked flask and was ultrasonically mixed to get uniform dispersion. Next, the three-necked flask containing the uniformly mixed dispersion was placed in a constant temperature water bath and was kept stirring. Both the left and right openings of the three-necked flask were sealed and the gas measuring device was connected through the middle opening. After the addition of AB solution, composed of 30 mg of AB and 0.2 mL of deionized water, the left opening of the three-necked flask was sealed again. The hydrogen generation rate from AB hydrolysis of AB was calculated by following equation:

$$\mathrm{TOF} = \frac{n_{\mathrm{H_2}}}{n_{\mathrm{catalyst}} t}, \quad (1)$$

where TOF is rate of hydrogen generation from AB hydrolysis ($\mathrm{min^{-1}}$), $n_{\mathrm{H_2}}$ is molar mass of the volume of

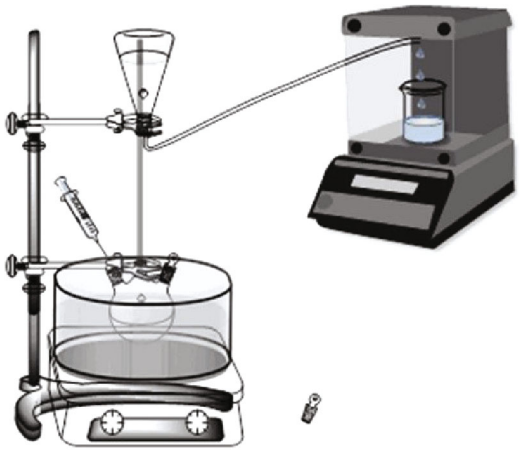

Fig. 2. The performance test apparatus for hydrogen generation from AB hydrolysis.

hydrogen generation (mol), $n_{catalyst}$ is molar mass of the catalyst (mol), t is reaction time (min). The term TOF was used to evaluate and compare the catalytic activity of PtNi(x : y)/FCNTs-D catalyst. It refers to the molar amount of hydrogen generation per unit time per unit of the catalyst.

The activation energy test of hydrogen generation from AB hydrolysis was used to measure the difficulty of the reaction in the presence of the catalyst. The hydrogen generation rate constant k was measured from the data obtained from the reaction under a series of water bath reaction temperature. The activation energy (E_a) was measured by using following equation:

$$\ln k = \ln A - \frac{E_a}{RT}, \quad (2)$$

where k is hydrogen generation rate constant, A is prereference factor, E_a is activation energy (kJ mol^{-1}), R is ideal gas constant (8.314 J mol^{-1} K^{-1}), T is reaction temperature (K).

The repeatability and durability tests for hydrogen generation were conducted by using five repeated cycle of catalytic activity. After each catalyst activity test cycle for hydrogen generation, the catalyst was washed and used again to study the hydrogen generation at 298 K.

RESULTS AND DISCUSSION

The morphology, the average Pt particle size and its distribution in all the PtNi(x : y)/FCNTs-D catalyst were studied by using transmission electron microscopy (TEM) (see Figs. 3a–3d and 3e–3h). It was found that highly dispersed nanoparticles were clearly loaded on the carboxylated carbon nanotubes. The average Pt particle size distribution in the PtNi(1 : 0)/FCNTs-D, PtNi(1 : 1)/FCNTs-D, PtNi(1 : 2)/FCNTs-D, and PtNi(1 : 4)/FCNTs-D catalysts was 1.35 nm (see Fig. 3e), 1.85 nm (see Fig. 3f), 1.95 nm (see Fig. 3g), and 1.95 nm (see Fig. 3h), respectively. The overall range of the average Pt particle size was in the range from 1.35 to 1.95 nm. The TEM analysis showed that the average Pt particle size was increased with the increase in Ni amount up to Pt : Ni ratio of 1 : 2. Upon further increase in Ni amount, for instance in case of PtNi(1 : 4)/FCNTs-D catalyst, the average Pt particle size was the same as to PtNi(1 : 2)/FCNTs-D catalyst. It showed that after a certain Pt to Ni ratio, there was no impact of Ni amount to the Pt particle size.

The X-ray diffraction (XRD) studies (see Fig. 4) showed two peaks at 25.8° and 42.8°, correspond to the (002) and (101) graphitic carbon reflections. Except afore mentioned two peaks, none of the analyzed catalytic sample (PtNi(x : y)/FCNTs-D at x : y = 1 : 1, 1 : 2, and 1 : 4) had shown any pure platinum, pure nickel and/or platinum-nickel alloy phase peaks.

To investigate the possible oxidation states and their association to the catalytic activity, all the studied catalysts were analyzed by using X-ray photoelectron spectroscopy (XPS). The results were shown in Fig. 5 and Table 1. Figure 5a was an overall comparison of the identified peaks of the all the four catalysts (PtNi(x : y)/FCNTs-D at x : y = 1 : 0, 1 : 1, 1 : 2, and 1 : 4). The peaks at 72.0, 284.5, 532.16, and 856.54 eV correspond to Pt 4f, C 1s, O 1s, and Ni 2p [16], respectively. To understand the different Pt and Ni oxidation states, each Pt and Ni corresponding peak in PtNi(x : y)/FCNTs-D catalyst was deconvoluted and results were shown in Figs. 5b and 5c. The peaks at 71.80 eV ($4f_{7/2}$) and 75.15 eV ($4f_{5/2}$) corresponded to Pt^0, peaks at 72.70 eV ($4f_{7/2}$) and 76.30 eV ($4f_{5/2}$) corresponded to Pt^{2+}, peaks at 74.90 eV ($4f_{7/2}$) and 78.10 eV

Table 1. Summary of the Pt and Ni oxidation states in PtNi(x : y)/FCNTs-D catalyst

x : y	Species (B.E., eV)/(area, %)					Element content, wt %	
	Pt^0	Pt^{2+}	Pt^{4+}	Ni^0	Ni^{2+}	Pt	Ni
1 : 0	72.01/55	72.93/32	75.10/13	—	—	2.92	0.00
1 : 1	71.89/51	72.73/25	74.99/24	852.64/4	856.65/96	2.15	1.16
1 : 2	71.44/49	72.32/33	74.50/18	852.67/1	856.59/99	2.92	6.63
1 : 4	71.52/52	72.44/38	74.76/10	851.91/1	857.00/99	2.10	3.30

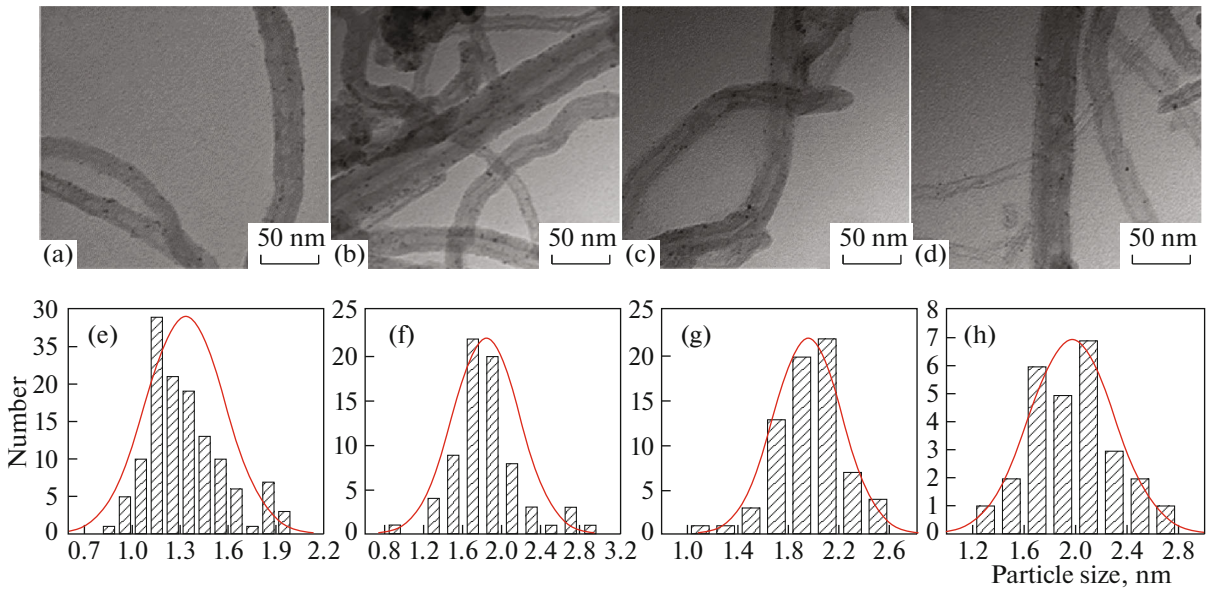

Fig. 3. TEM images of PtNi(x : y)/FCNTs-D catalysts and its particle size distribution; x : y= (a, e) 1 : 0, (b, f) 1 : 1, (c, g) 1 : 2, (d, h) 1 : 4.

($4f_{5/2}$) corresponded to Pt^{4+}. The peaks at 69 eV corresponded to Ni 3p (assigned to $Ni(OH)_2$ [17]), peaks at 852.35 eV ($2p_{3/2}$) and 869.75 eV ($2p_{1/2}$) corresponded to Ni^0 and peaks at 856.65 eV ($2p_{3/2}$) and 874.85 eV ($2p_{1/2}$) corresponded to Ni^{2+}. The overall comparison of present oxidation states of Pt and Ni were summarized in Table 1. Interestingly, the Ni^{2+} peaks were weighted 96% of the total other Ni peaks. In addition, with the increase in Ni amount in catalyst recipe, the peak position of Pt^0 began to shift to lower binding energy (for instance, see the Ni peaks in PtNi(1 : 2)/FCNTs-D catalyst (Fig. 5c). In all studied catalytic samples, the Pt^0 peaks was accounted ~50% of the total peak—a clear indication of Pt metal presence in its simplest form. In summary, the Pt^0, Pt^{2+}, Pt^{4+}, and Ni^{2+} species were found in PtNi(x : y)/FCNTs-D catalysts.

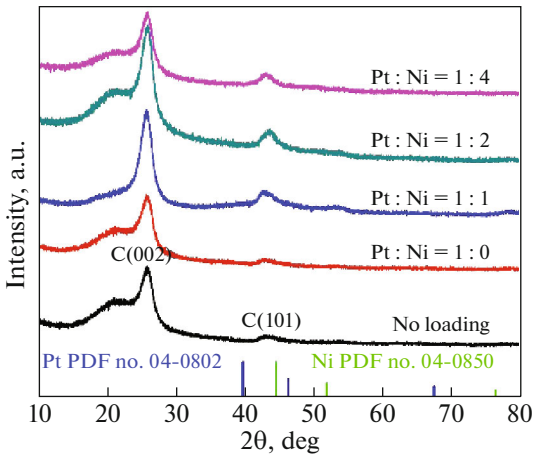

Fig. 4. XRD patterns of PtNi(x : y)/FCNTs-D catalysts and carboxylated carbon nanotubes.

Figure 6a was the comparison of catalytic activity and the amount of hydrogen generation (in terms of TOF) from AB hydrolysis of all the studied PtNi(x : y)/FCNTs-D catalysts at room temperature (298 K). The catalytic activity of PtNi(1 : 0)/FCNTs-D was 165 mol_{H_2} min^{-1} mol_{pt}^{-1} (see Fig. 6b), which was similar to the catalytic activity of the pure platinum catalyst reported previously [18]. Whereas, the catalytic activity of the PtNi(1 : 1)/FCNTs-D catalyst was 476 mol_{H_2} min^{-1} mol_{pt}^{-1}, which was far higher as to that of PtNi(1 : 0)/FCNTs-D catalyst. The catalytic activity of the PtNi(1 : 2)/FCNTs-D and the PtNi(1 : 4)/FCNTs-D catalysts was 597 and 377 mol_{H_2} min^{-1} mol_{pt}^{-1}, respectively. In comparison, the catalytic activity of the PtNi(1 : 2)/FCNTs-D was the highest as to the other studied PtNi(x : y)/FCNTs-D catalysts. It clearly showed that the presence of Ni in the catalyst composition favorably impacted to enhance the catalytic activity of PtNi(x : y)/FCNTs-D catalyst. However, an optimum Pt : Ni was key aspect and in this study it was 1 : 2. Beyond this ratio, the catalytic activity was lowered.

To study the effect of reaction temperature to the catalytic activity and amount of hydrogen generation, the best PtNi(1 : 2)/FCNTs-D catalyst and was tested further at different reaction temperatures of 298, 303, 308, and 313 K (see Fig. 7a). For each reaction temperature, the value of hydrogen generation rate con-

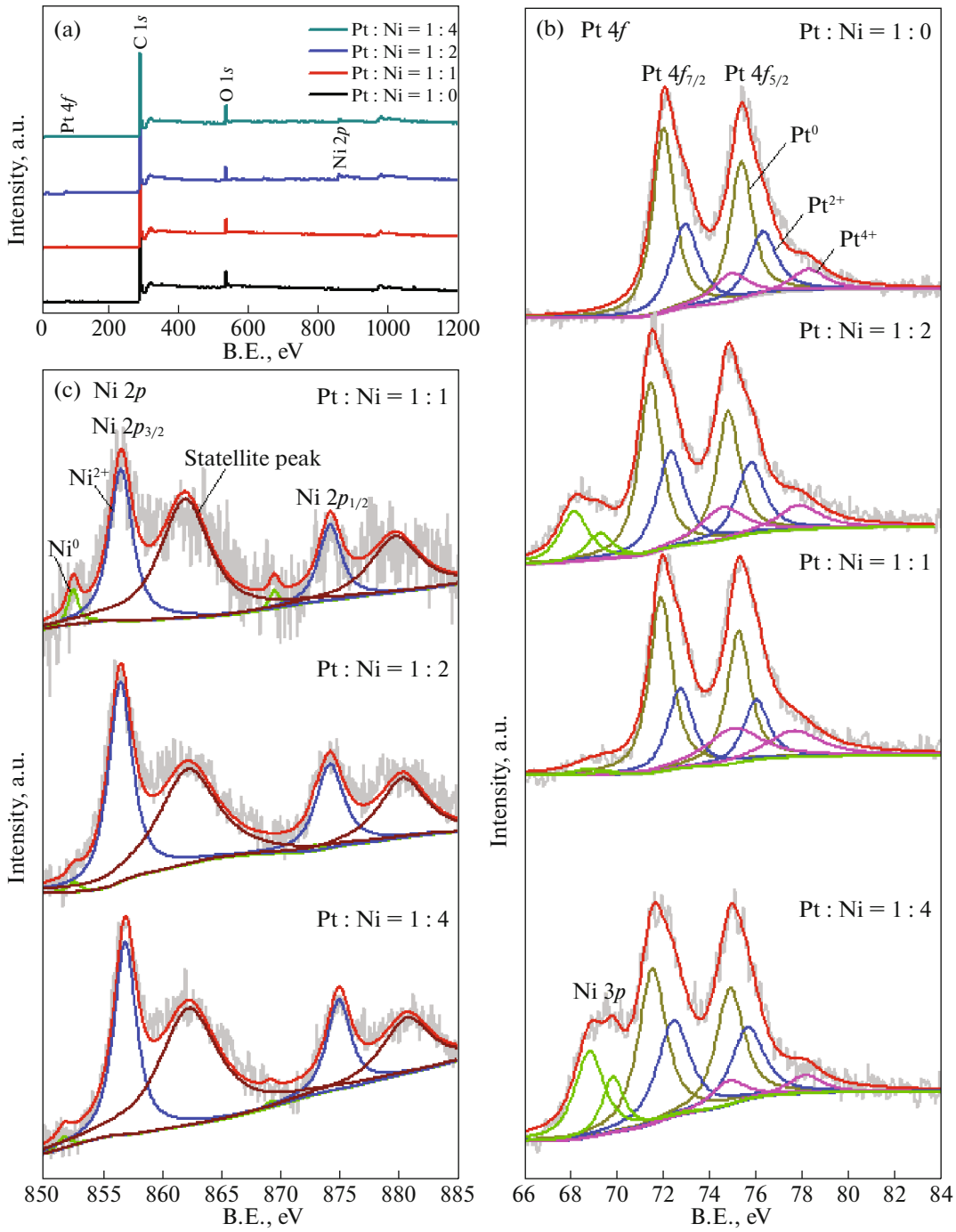

Fig. 5. X-ray photoelectron spectrum of PtNi(x : y)/FCNTs-D (a) comparison of full spectrum, (b) Pt 4*f* spectrum, (c) Ni 2*p* spectrum.

stant k was calculated. The value of activation energy E_a was calculated using Arrhenius equation (see Fig. 7b). The obtained results were summarized in Fig. 7b.

The catalytic activity performance comparison of best PtNi(1 : 2)/FCNTs-D catalyst to the reported available literature was summarized in Table 2. Based on it, the PtNi(1 : 2)/FCNTs-D catalyst need lowest activation energy (32 kJ/mol) in comparison to the Pt/CNTs-O-HT, PEI–GO/$Pt_{0.17}Co_{0.83}$, $Ni_{0.33}$@$Pt_{0.67}$/C, $Co_{0.32}$@$Pt_{0.68}$/C, and STA-Pt/CNT catalysts. The lowered E_a in AB hydrolysis for the PtNi(1 : 2)/FCNTs-D catalyst was an indication Pt : Ni ratio in the catalyst composition assisted to

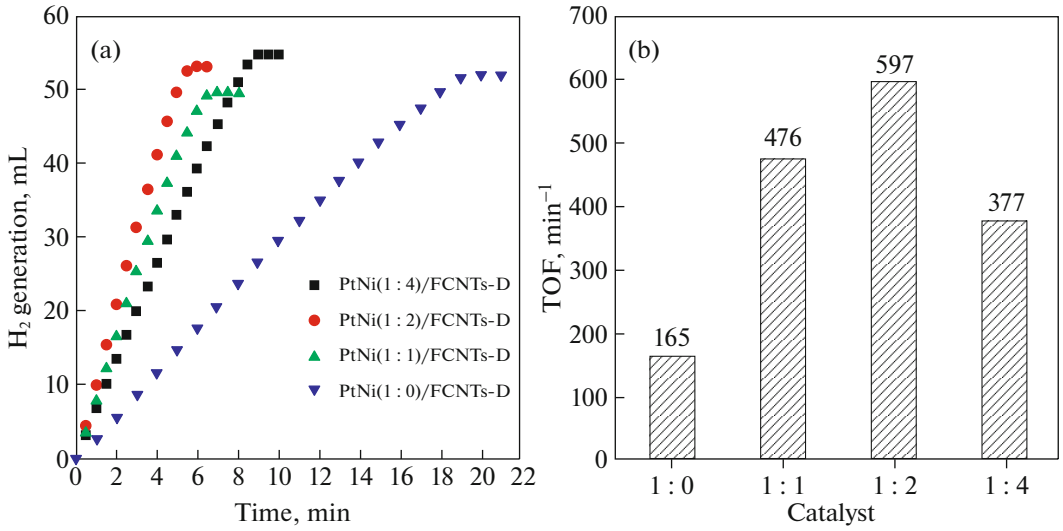

Fig. 6. Comparison of (a) catalytic activity and (b) hydrogen generation from AB hydrolysis of the PtNi(x : y)/FCNTs-D catalysts.

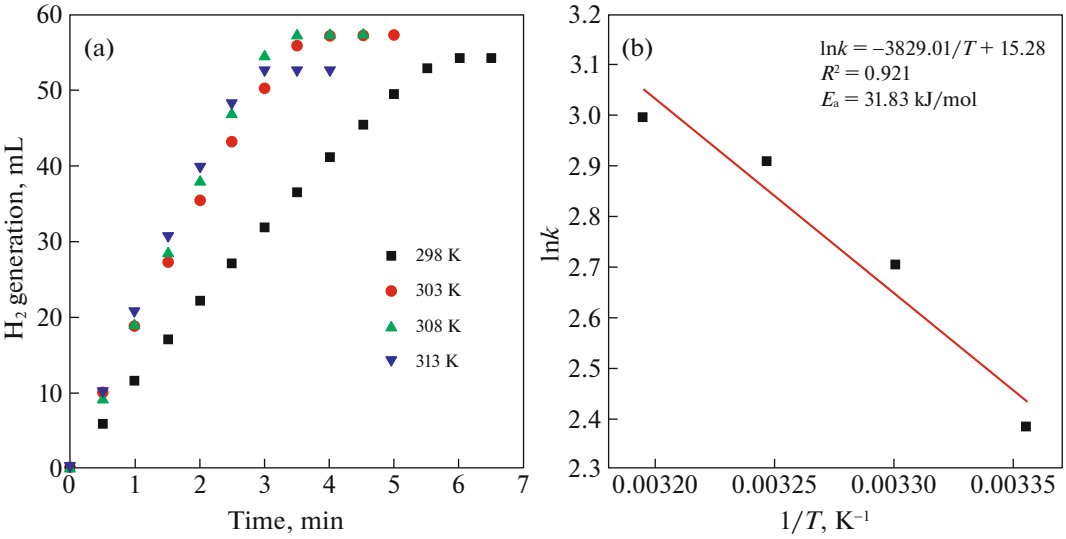

Fig. 7. (a) Catalytic activity test of PtNi(1 : 2)/FCNTs-D catalyst for AB hydrolysis at different temperatures and (b) Arrhenius equation fitting curve of PtNi(1 : 2)/FCNTs-D catalyst.

shift the thermodynamic equilibrium to lower side, which favorably promoted the catalytic reaction [19]. In general, the PtNi(1 : 2)/FCNTs-D catalyst had shown highest amount hydrogen generation from AB hydrolysis at 298 K.

To investigate the repeatability, the best PtNi(1 : 2)/FCNTs-D catalyst was tested repeatedly for five repeats(R1, R2, R3, R4, and R5). The amount of H_2 generation in R1, R2, R3, R4, and R5 was 597, 372, 354, 290, and 287 mol_{H_2} min^{-1} mol_{pt}^{-1}, respectively (see Fig. 8). After the first repeat (R2), the amount of H_2 generation from AB hydrolysis decreased to 62%. After the fifth repeat (R5), the amount of H_2 generation from AB hydrolysis reduced to 48% to the initial catalytic activity. However, even after fifth repeat cycle (R5), the catalytic activity of the best PtNi(1 : 2)/FCNTs-D catalyst was higher as to the catalytic activity of the pure platinum catalyst (PtNi(1 : 0)/FCNTs-D). In general, the catalytic gradually decreased with the increase in the number of repeat test. The decrease catalytic activity for H_2 generation form AB hydrolysis was due to change in morphology intertwined of carboxylated carbon nanotubes and the agglomeration of the nanoparticles due to their shedding during cleaning process (see Fig. 9).

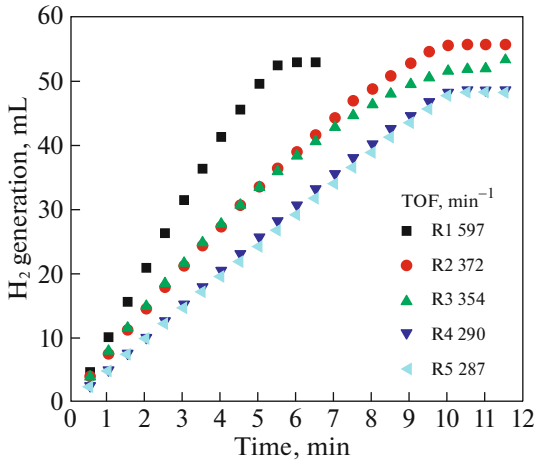

Fig. 8. The repeatability test of PtNi(1 : 2)/FCNTs-D for AB hydrolysis.

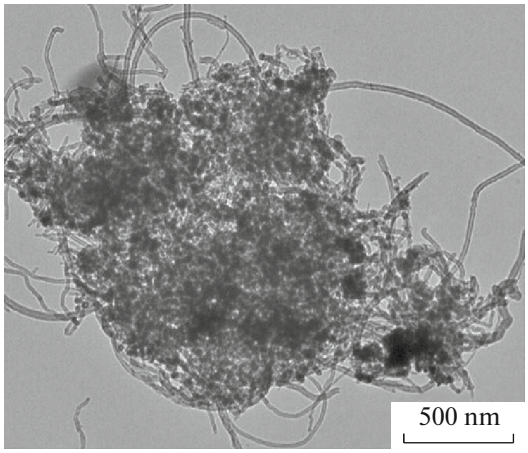

Fig. 9. TEM image of PtNi(1 : 2)/FCNTs-D catalyst after the fifth use in AB hydrolysis.

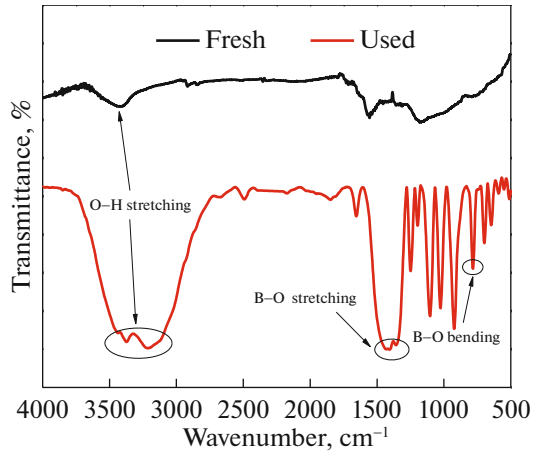

Fig. 10. The comparison of infrared spectra of PtNi(1 : 2)/FCNTs-D catalyst before and after AB hydrolysis.

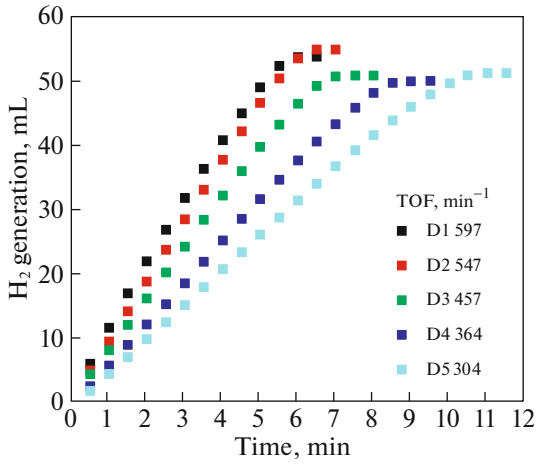

Fig. 11. The durability test of PtNi(1 : 2)/FCNTs-D catalyst for AB hydrolysis.

To investigate it further, an infrared analysis of PtNi(1 : 2)/FCNTs-D was performed before and after the AB hydrolysis (see Fig. 10). It was found that the used catalyst had many new characteristic peaks. Among new peaks, the peaks at 3200–3400 cm^{-1} corresponded to O–H stretching peak, the peak at 1450 cm^{-1} corresponded to B–O stretching peak, the peak at 780 cm^{-1} corresponded to B–O bending peak [25]. The peaks were attributed to the BO_2^- and/or other by-products during AB hydrolysis.

In addition to the repeatability, the PtNi(1 : 2)/FCNTs-D catalyst was tested for its durability for H_2 generation from AB hydrolysis. The durability of the best catalyst was tested 5 times (D1, D2, D3, D4, and D5). The results were shown in Fig. 11. After the second reaction (D2), the catalytic activity remained almost the same as to the first reaction (D1). However, the catalytic activity was decreased slightly in the third reaction (D3; TOF = 457 mol_{H_2} min^{-1} mol_{pt}^{-1}), which was about 77% of the initial activity. After the fifth cycle (D5), the amount of H_2 produced was 304 mol_{H_2} min^{-1} mol_{pt}^{-1} – approximately to 51% of the initial catalytic activity, which was still higher than the activity of the pure platinum catalyst PtNi(1 : 0)/FCNTs-D.

Based on the combined with TEM and XRD analysis, it was clear that bimetallic Pt–Ni nano-catalysts were successfully supported on the carbon nanotubes. None of the prepared PtNi(x : y)/FCNTs-D catalysts showed pure platinum phase or pure nickel phase or platinum-nickel alloy. This attributed to the small

Table 2. The performance comparison of platinum-based catalysts in hydrogen generation from AB hydrolysis

Catalyst	T, K	TOF, min^{-1}	E_a, kJ/mol	Ref.
PtNi(1 : 2)/FCNTs-D	298	597	32	This work
Pt/CNTs-O-HT	298	468	—	[9]
Pt/γ-Al_2O_3	298	222	21	[20]
PEI–GO/$Pt_{0.17}Co_{0.83}$	298	378	52	[21]
$Ni_{0.33}$@$Pt_{0.67}$/C	298	167	33	[22]
$Co_{0.32}$@$Pt_{0.68}$/C	298	148	42	[23]
STA-Pt/CNT	298	517	39	[24]

sized nanoparticles loaded on the carboxylated carbon nanotubes and/or amorphous shape particles. The catalyst PtNi(1 : 2)/FCNTs-D showed the highest catalytic activity in comparison to the PtNi(1 : 0)/FCNTs-D, PtNi(1 : 1)/FCNTs-D, and PtNi(1 : 4)/FCNTs-D catalyst. According to the available literature and experimental results, this phenomenon could be governed by the Sabatier principle. Due to the availability of the best free adsorption energy on the catalytic surface either to reactants and/or reaction intermediates, thus it exhibited the best catalytic activity [26]. In addition, if the binding energy of the intermediate was too weak, it would be difficult to activate the substrate on the catalyst surface and vice-versa. According to the XPS characterization, there an electron transfer took placed from Ni to Pt atoms, which caused the chemical shift of Pt element to move negatively. When the amount of nickel precursor was increased to Pt : Ni = 1 : 2, the binding energy of Pt^0 decreased, and the catalytic activity got increased. Whereas, after increasing Pt : Ni ration to 1 : 4, the binding energy of Pt^0 began to increase, and due to which the catalytic activity was decreased. It indicated that the lower the binding energy of Pt^0, the higher the catalytic activity, and the catalyst had the best free energy of adsorption. Based on TEM and IR analysis, the decrease in catalytic activity of PtNi(1 : 2)/FCNTs-D after its multiple use could be due to the agglomeration of the nanoparticles, which lead to the lesser availability of the active sites.

CONCLUSIONS

In summary, a facile method for the preparation of bimetallic Pt–Ni nano-catalysts supported on the carbon nanotubes is beneficial to improve the catalytic activity for hydrogen generation from AB hydrolysis. In addition, the presence of carbon nanotubes in the catalyst composition improves the dispersion and stability of the nanoparticles. The availability of more active sites and lowered binding energy of Pt^0 in PtNi(1 : 2)/FCNTs-D catalyst, lead to the increased catalytic activity of H_2 generation from AB hydrolysis at room temperature as to the other studied PtNi(1 : 0)/FCNTs-D, PtNi(1 : 1)/FCNTs-D, and PtNi(1 : 4)/FCNTs-D catalysts. In brief, a new synthesis strategy to design bimetallic catalysts for highly efficient hydrogen generation is the key aspect of this study.

ACKNOWLEDGMENTS

This work was supported by the Local Science and Technology Development Fund Projects Guided by the Central Government of China (no. 2021ZYD0060), the Science and Technology Project of Southwest Petroleum University (no. 2021JBGS03), and the Chengdu International Science and Technology Cooperation Fund (2020GH0200069HZ).

DATA AVAILABILITY STATEMENT

The data that support this study are available in the article and accompanying online supplementary material.

CONFLICT OF INTEREST

The authors declare that they have no conflicts of interest.

REFERENCES

1. Y. Du, Y. Shen, Y. Zhan, et al., Chin. Chem. Lett. **28**, 1746 (2017).
2. L. M. Kustov, A. N. Kalenchuk, and V. I. Bogdan, Russ. Chem. Rev. **89**, 897 (2020).
3. S. Yu, G. Jing, S. Li, et al., Int. J. Hydrogen Energy **45**, 6757 (2020).
4. G. Sandrock, J. Reilly, J. Graetz, et al., J. Alloys Compd. **421**, 185 (2006).
5. A. Züttel, P. Wenger, S. Rentsch, et al., J. Power Sources **118**, 1 (2003).
6. A. Mehranfar and M. Izadyar, RSC Adv. **5**, 49159 (2015).
7. R. Kumar, A. Karkamkar, M. Bowden, et al., Chem. Soc. Rev. **48**, 5350 (2019).
8. F. H. Stephens, V. Pons, and R. T. Baker, Dalton Trans. **36**, 2613 (2007).
9. W. Chen, J. Ji, X. Duan, et al., Chem. Comm. **50**, 2142 (2014).
10. Y. Ge, Z. H. Shah, X. Lin, et al., ACS Sustain. Chem. Eng. **5**, 1675 (2017).
11. J. Kang, T. Chen, D. Zhang, et al., Nano Energy **23**, 145 (2016).
12. S. Rej, C. F. Hsia, T. Y. Chen, et al., Angew. Chem. Int. Ed. **128**, 7338 (2016).
13. H. Yen, Y. Seo, S. Kaliaguine, et al., ACS Catal. **5**, 5505 (2015).
14. A. N. Kalenchuk, V. I. Bogdan, L. M. Kustov, et al., Fuel **280**, 118625 (2020).
15. A. N. Kalenchuk, V. I. Bogdan, L. M. Kustov, et al., Fuel Process. Technol. **169**, 94 (2018).

16. L. Ma, Q. Zhang, C. Wu, et al., Anal. Chim. Acta **1055**, 17 (2019).
17. J. San Choi, C. W. Ahn, J. Bae, et al., Curr. Appl. Phys. **20**, 102 (2020).
18. Q. Xu and M. Chandra, J. Alloys Compd. **446**, 729 (2007).
19. F. Fu, C. Wang, Q. Wang, et al., J. Am. Chem. Soc. **140**, 10034 (2018).
20. M. Chandra and Q. Xu, J. Power Sources **168**, 135 (2007).
21. M. Li, J. Hu, Z. Chen, et al., RSC Adv. **4**, 41152 (2014).
22. X. Yang, F. Cheng, J. Liang, et al., Int. J. Hydrogen Energy **36**, 1984 (2011).
23. X. Yang, F. Cheng, Z. Tao, et al., J. Power Sources **196**, 2785 (2011).
24. W. Fu, C. Han, D. Li, et al., J. Energy Chem. **41**, 142 (2020).
25. C. Liu, Y. Wu, C. Chou, et al., Int. J. Hydrogen Energy **37**, 2950 (2012).
26. U. B. Demirci and F. Garin, J. Alloys Compd. **463**, 107 (2008).